Geophysical Research Letters

RESEARCH LETTER
10.1029/2017GL076812

Key Points:
- Body-to-surface wave conversions at the U.S. continental margin can be observed at USArray
- Two-dimensional spectral element simulations can generate *S*-to-Rayleigh wave scattering
- The scattered wave train is amplified locally by 3-D effects

Supporting Information:
- Supporting Information S1

Correspondence to:
J. Buehler,
buehleja@gmail.com

Citation:
Buehler, J. S., Mancinelli, N. J., & Shearer, P. M. (2018). *S*-to-Rayleigh wave scattering from the continental margin observed at USArray. *Geophysical Research Letters*, *45*, 4719–4724. https://doi.org/10.1029/2017GL076812

Received 14 DEC 2017
Accepted 27 APR 2018
Accepted article online 10 MAY 2018
Published online 22 MAY 2018

©2018. American Geophysical Union. All Rights Reserved.

S-to-Rayleigh Wave Scattering From the Continental Margin Observed at USArray

J. S. Buehler[1], **N. J. Mancinelli**[2], **and P. M. Shearer**[1]

[1]Scripps Institution of Oceanography, University of California, San Diego, La Jolla, CA, USA, [2]Department of Earth, Environmental and Planetary Sciences, Brown University, Providence, RI, USA

Abstract We show examples of teleseismic *S* waves from western Pacific earthquakes converting to surface waves near the western U.S. coastline. Many of these events originate in the Tonga-Samoa region. We observe these surface wave conversions at USArray stations at relatively long periods (>10 s). The amplitudes vary considerably from station to station and appear highly amplified in the Yellowstone region. Two-dimensional spectral element simulations successfully generate scattered Rayleigh waves from incident *SV* waves and models with surface topography at the coastline and crustal thickness variations across the margin, although simple models cannot explain the large Rayleigh wave amplitudes (greater than the direct *S* wave amplitude) observed in some regions, suggesting that the wave train is amplified by local structure or 3-D focusing effects.

Plain Language Summary We show new observations of body-to-surface wave conversions at the U.S. continental margin observed with USArray. Simulation results show how simple surface topography at the coastline can successfully generate scattered Rayleigh waves from incident *SV* waves. These converted surface waves may be an important source of signal-generated noise in continental seismology, in particular in studies of seismic phases and parts of the wavefield between direct *S* and later-arriving surface waves from the source.

1. Introduction

The high station density of USArray permits exploring the teleseismic wavefield in great detail (e.g., Foster et al., 2014; IRIS DMC, 2010; Sun & Helmberger, 2011). Here we show that USArray record sections from distant earthquakes often contain strong coherent wave trains following the direct *S* wave. These wave trains are especially prominent in long-period seismograms for paths arriving from the west. The feature is visible most clearly on the vertical component, appears dispersive, and travels with an apparent group velocity of ~3.0 km/s, consistent with *S*-to-Rayleigh wave conversions.

Body-to-surface wave scattering due to surface topography has been studied since the 1960s (Levander, 1990). Converted surface waves similar to our USArray observations have been observed from scattered *P* waves at the Japan Trench (Maeda et al., 2014), at the Pacific Trench of Mexico (Dominguez et al., 2011), for deep events near Australia (Furumura et al., 1998), and most recently by Yu et al. (2017) who reported *SH*-to Love wave scattering off the Southern California Continental Borderland for deep events in the Fiji region. It is important to be aware of these large-amplitude arrivals cutting across body wave phases, as they could interfere with analyses of direct or converted phases in this part of the wavefield, causing problems for migration, back projection, or attenuation tomography. In fact, we discovered this wave train while searching for possible contamination in long-period reflections from mantle discontinuities.

Here we describe observations of *S*-to-Rayleigh wave conversions at the U.S. continental margin and investigate the potential origin of this wave train. We focus on teleseismic events and show examples of record sections with clear observations of scattered wave arrivals. We investigate the effect of the slope and height of the continental margin on the generation of these surface waves using 2-D spectral element modeling and compare our observations with other surface wave amplification studies.

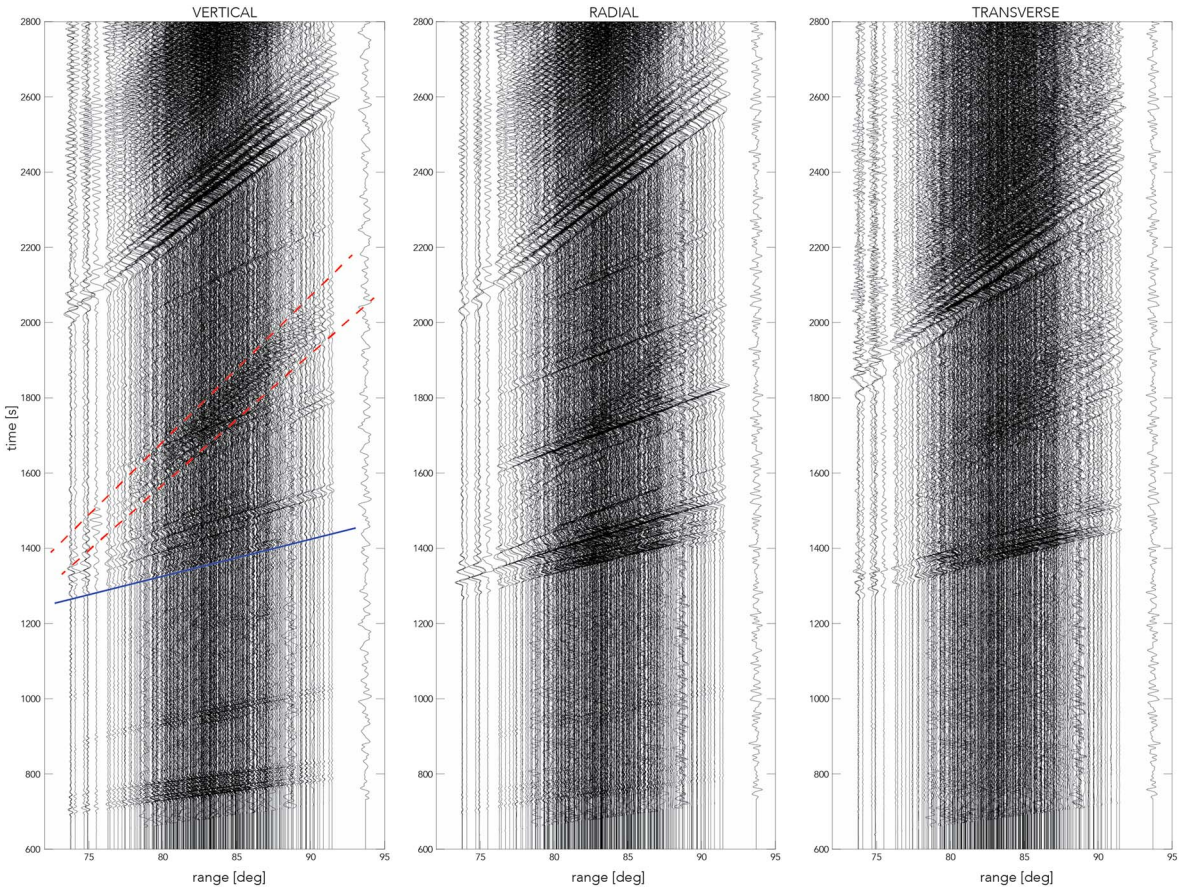

Figure 1. USArray record section for a *Mw* 6.6 Samoa Islands region earthquake on 30 August 2009, showing the vertical, radial, and transverse components. The *S* wave arrival is indicated by the blue line on the vertical component; the scattered Rayleigh waves are bounded by the red dotted lines, with apparent velocities between 2.7 and 3.2 km/s.

2. Observations of Scattered Surface Waves at USArray

Our database consists of global teleseismic events recorded by USArray between the years 2004 and 2014 with hypocenter depths less than 50 km. One of the clearest examples of a scattered wave train we found is for an event in the Samoa Islands Region (Figure 1). This *Mw* 6.6 earthquake occurred at 14.5 depth km, as a normal faulting event in the outer rise of the Tonga subduction zone. In seismograms at greater than 74° range, a slower-propagating wave train with amplitudes exceeding those of direct *S* for some stations starts emerging between 1,400 and 2,000 s and cuts across the faster-propagating *SS* wave. The seismograms are low-pass filtered at 10 s. We find that the scattered field is generally visible at periods between 10 and ~50 s, but the wave train amplitudes are diminished at longer periods, in contrast to the regular surface waves (Figure 2). The signal becomes much more visible by plotting only the seismograms with large amplitudes in the scattered surface wave time window (Figure 3a).

While most of the events with a clear converted surface wave train appear to have origins in the Fiji-Samoa region, we find examples from earthquakes at other subduction zones, such as the Japan and Marianas trenches (see supporting information figures for more example record sections). We attempted a systematic search for events that generate these converted surface wave arrivals by stacking envelope amplitudes in the expected time window, normalized to the maximum direct *S* wave amplitude, for each event. We define the stacking window by finding the coastal point along each great-circle path and estimating the arrival time of the scattered *S* wave as the sum of the direct *S* wave time for the epicenter-to-coast distance and the surface wave time for the coast-to-station distance. However, it is challenging to avoid obtaining many false high-amplitude results, given that other phases, such as *SS*, are interfering and we are assuming that the scattering lies along the great-circle path. We also tried the approach of Maeda et al. (2014) who used coherence analysis to remove the direct wave packets from the seismograms. They stack seismograms from stations

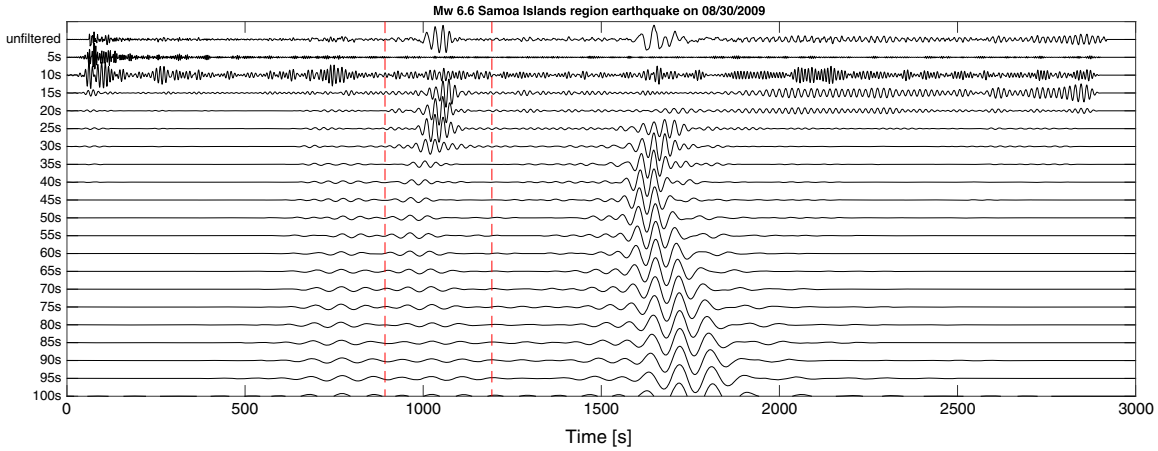

Figure 2. Seismograms from a *Mw* 6.6 Samoa Islands region earthquake on 30 August 2009 recorded at station H18A, narrow band filtered for a range of periods. Scattered surface wave arrival window is indicated with red dashed lines.

in a zone between isodistance curves according to great-circle paths and then remove the stacked trace from individual seismograms, assuming that the wavefronts from a scattering source from a different direction would not be muted. However, in our case, the surface wave train also seems to stack coherently, suggesting not a single point of origin but rather a conversion to surface wave energy at multiple locations along the coast. Although we did not find an automatic detection approach that worked reliably, we were able to identify 21 earthquakes that show a converted surface wave train with varying clarity in the USArray data.

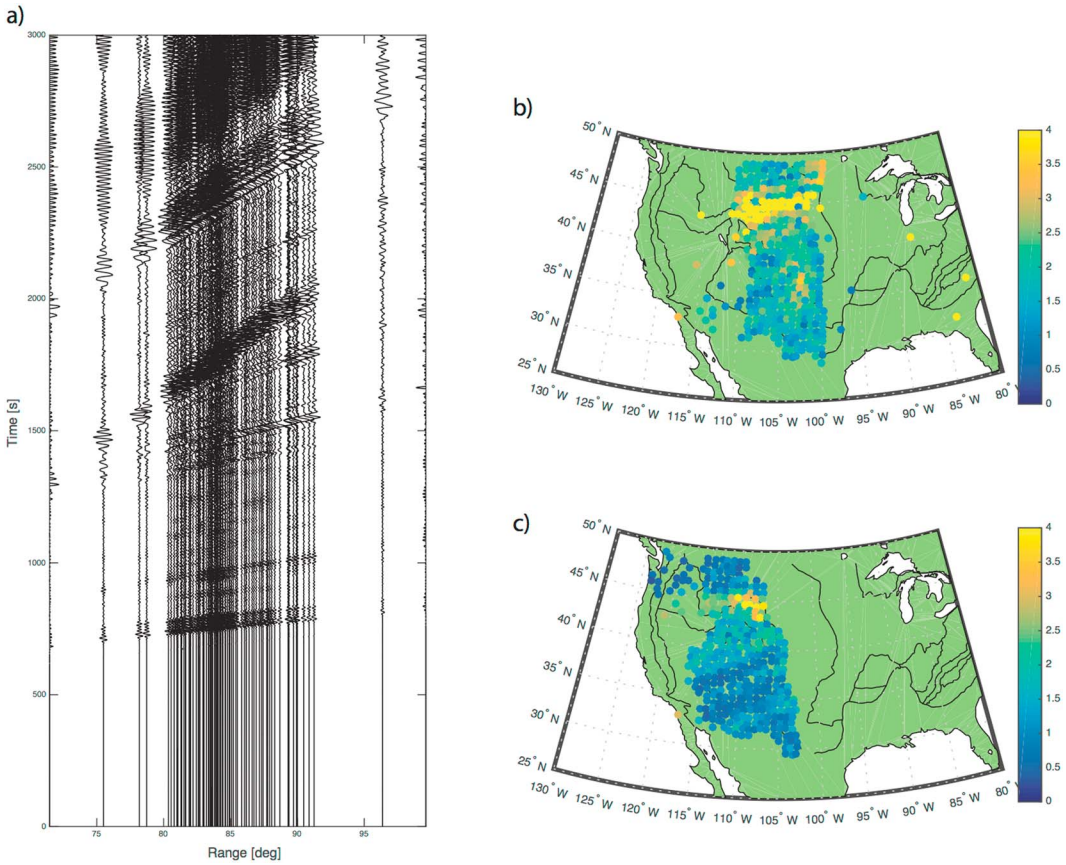

Figure 3. (a) A subset of the record section in Figure 1, plotting only high-amplitude scattered surface waves. (b) Map view of maximum scattered surface wave amplitude at each station. (c) Same as (b) for a *Mw* 6.0 Tonga Islands earthquake on 19 August 2008.

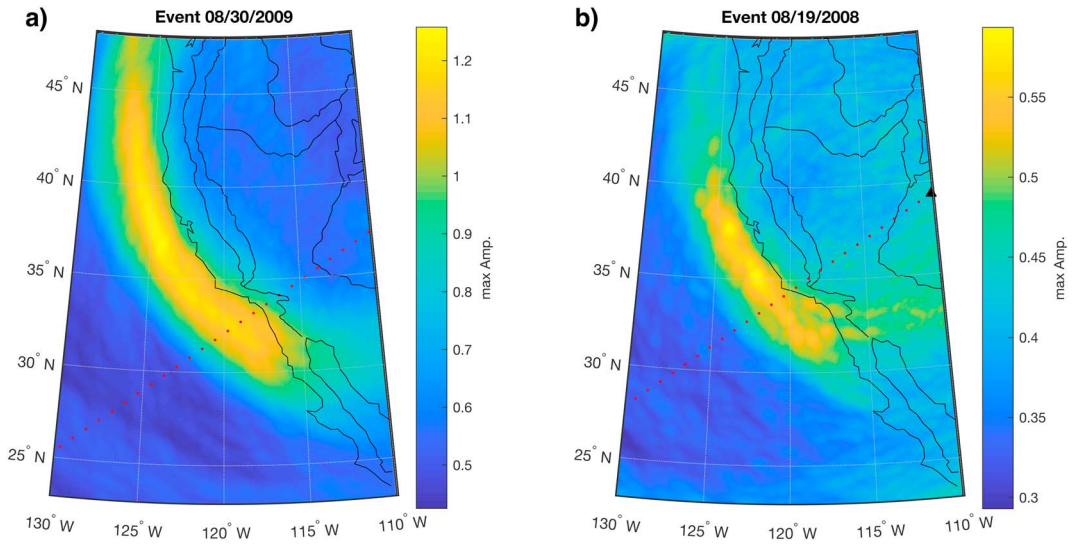

Figure 4. Grid amplitudes after migrating each seismogram to its possible scatterer locations. (a) For the *Mw* 6.6 Samoa Islands region earthquake on 30 August 2009 and (b) for the *Mw* 6.0 Tonga Islands earthquake on 19 August 2008. The red dotted line shows the great-circle path from the event to the centroid location of the USArray stations.

Plotting scattered wave amplitudes at the station locations shows interesting structural patterns. Examples for two different earthquakes are shown in Figures 3b and 3c. Most of the large amplitudes are recorded at stations around the Yellowstone region, where surface wave amplification has previously been observed (Eddy & Ekström, 2014; Lin et al., 2012). Lin et al. (2012) found the strongest amplification across the Snake River Plain and the Rocky Mountains for Rayleigh waves with a period of 60 s, and, in better agreement with our study, Eddy and Ekström (2014) saw strong amplification to the east of the Snake River Plain for shorter-period waves. Figure 2b additionally shows a striped pattern south of the high-amplitude region. Similar patterns have been noted in other USArray surface wave studies and attributed to interference by structural variations (Lin & Ritzwoller, 2011).

Next we try to constrain the scatterer locations by migrating each signal to potential scattering points. The arrival of the incident waves from the west suggests that the converted energy is generated at the continental margin. We define a 2-D grid along the western margin and compute direct *S* wave times to each grid node, then compute surface wave times from each grid node to each station (along great-circle paths), using an average propagation velocity of 3.0 km/s. We stack the envelopes of seismograms from all stations according to the sum of both times for each grid node, using a tapered 160 s window (80 s before and after the theoretical time from the trial scatterer location). We then plot the maximum amplitude of the stacked traces in the time window for each grid location. Figure 4 shows that there does not appear to be a single scattering location and that the waves are scattered at multiple points along the margin, in agreement with earlier coherence observations. We also do not observe circular wavefronts traveling across USArray, as might be expected from strong scattering in a single location (however, the station spacing might be too large to observe clear evidence). For the few events from the Northern Hemisphere, the apparent scattering location is west of the coastline, near the Juan de Fuca plate boundary ridge (see supporting information figures), suggesting that perturbations in the upper lithosphere and crust could be another important factor, in addition to topography, in the generation of scattered surface waves.

3. Scattered Waves Simulation

We use SPECFEM2D (Chaljub et al., 2007; Komatitsch et al., 2012) to investigate the effect of surface topography at the coastline on incident *S* plane waves (Figure 5). The ocean-continent surface topography is parameterized as an error function (see supporting information to see how this compares to realistic topography), and we explore what rise times (Δx) and amplitudes (Δz) of the function are needed to produce surface wave conversions that match our observations. To broadly sample the parameter space, we vary Δx from 3 to 100 km and Δz from 2.5 to 40 km, resulting in slopes from 0.05 to over 1 (unrealistic) in a uniform elastic half-space ($\alpha = 7.92$ km/s, $\beta = 4.40$ km/s). 150 receivers are evenly distributed 75–1,100 km

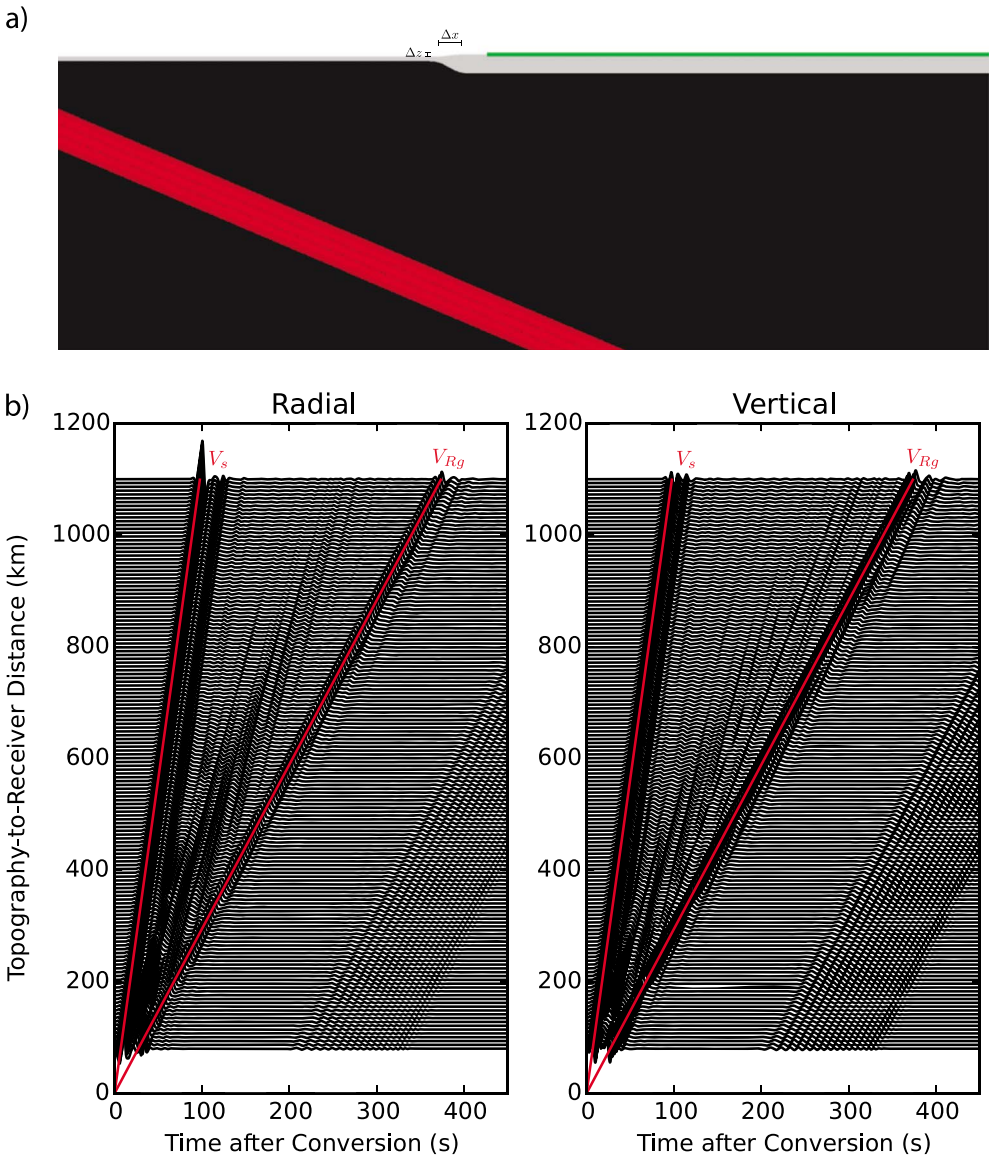

Figure 5. (a) Setup of 2-D synthetic experiment. Incident *SV* plane wave (red) propagating from left to right about to arrive at the continental margin. Green line indicates receiver array. (b) Synthetic seismogram record sections. Direct *S* and scattered Rayleigh wave are indicated with red lines.

from the continental margin. The incident wave packet is a Ricker wavelet with a dominant period of 10 s; it strikes the free surface at an angle of 23° from the horizontal. As the plane wave crosses the rise in topography, a scattered wave is generated with a moveout in close agreement with the theoretical value for a Rayleigh wave propagating on the edge of an elastic half-space. In general, the steeper the rise, the larger the amplitudes of the generated converted wave, although the absolute lengths of Δx and Δz matter as well (a bigger feature leads to larger converted amplitudes). The generated surface waves are nondispersive, an effect of the uniform elastic half-space used in the model.

Next we add a crustal layer ($\alpha = 5.66$ km/s, $\beta = 3.20$ km/s), 8 km thick over the ocean and 45 km thick on the continent side (Figure 5a). The vertical relief on the free surface is set to 5 km over distances ranging from 5 to 25 km. The simulation results again show that the *S*-to-Rayleigh phase is present and follows the appropriate moveout (Figure 5b). The second set of surface waves coming well after the other phases is caused by edge effects of the model (see supporting information for model snapshots of the wave propagation). Generally, the scattered wave amplitude increases with Δz and slope, but it is difficult to generate amplitudes larger than 1 (with respect to direct *S* on the vertical component) with Earth-like topography parameters. A crustal model

that transitions abruptly (i.e., $\Delta x = 0$) from oceanic to continental thickness helps generate amplitudes closer to 1 (0.75–1.01), but the slope of topography on the free surface still must be unrealistically large (0.2–1.0).

Overall we find that the synthetic amplitudes are consistently smaller than the largest observed surface wave amplitudes, and simple surface topography models are not capable of generating amplitudes larger than that of direct *S*. The observed amplitudes vary considerably from station to station, suggesting that factors other than the coastal topography amplify the scattered wave train, such as local site and/or focusing effects. The wavefield simulations suggest that the frequency content of the scattered wave is controlled by two factors: the wavelength of topography and the change in crustal thickness across the margin. Although the former mechanism likely plays an important role, we emphasize the latter because models with abrupt changes in crustal thickness generate conversions with a frequency dependence similar to what we observe—even in the absence of surface topography (see supporting information). The following argument provides intuition for this result. At intermediate periods (10–50 s) the Rayleigh wave is most sensitive to structure of the lower crust and uppermost mantle, so scattering preferentially occurs within that period band. At longer periods (>50 s), however, the Rayleigh waves average over a broad depth range, so the relative impact of crustal thickness variations is lessened. At periods shorter than 10–20 s, our idealized models diverge from reality as the presence of the water column significantly influences short-period Rayleigh wave propagation in the oceans (e.g., Harmon et al., 2007). Future work should thoroughly explore the relative importance of the water column in this scattering process.

4. Summary

We have documented strong *S*-to-Rayleigh wave converted energy from the U.S. continental margin at USArray stations. Most of these observations are from subduction zone earthquakes in the Tonga region, at epicentral distances from 70° to 100°. The observed scattered wave amplitudes vary considerably from station to station, with the largest amplitudes observed in the Yellowstone region. Two-dimensional scattered wave simulations demonstrate that *S*-to-Rayleigh wave conversions are possible with simple models of surface topography at the continental margin but cannot replicate the largest observed amplitudes, implying the importance of 3-D effects. These converted surface waves may be an important source of signal-generated noise in continental seismology, in particular in studies of seismic phases and parts of the wavefield between direct *S* and later-arriving surface waves from the source. The conversions are easy to see in USArray data because of the high station density but are likely present for other continental geometries as well.

Acknowledgments
We thank two anonymous reviewers for their constructive comments that helped to improved this manuscript. Funding for this work was provided by NSF grants EAR-1358510 and EAR-1620251. We thank IRIS for data access and products. For providing access and support for SPECFEM2D, we thank the Computational Infrastructure for Geodynamics (http://geodynamics.org) which is funded by the National Science Foundation under awards EAR-0949446 and EAR-1550901. The wavefield simulations were conducted using computational resources and services at the Center for Computation and Visualization, Brown University.

References

Chaljub, E, Komatitsch, D., Vilotte, J.-P., Capdeville, Y., Valette, B., & Festa, G. (2007). Spectral-element analysis in seismology. *Advances in Wave Propagation in Heterogenous Earth*, *48*, 365–419. Elsevier.

Dominguez, L. A., Sanchez-Sesma, F. J., & Davis, P. M. (2011). Scattering of teleseismic body waves by the lateral crustal heterogeneity at the Pacific Trench of Mexico. *Bulletin of the Seismological Society of America*, *101*(3), 1281–1290. https://doi.org/10.1785/0120100181

Eddy, C. L., & Ekström, G. (2014). Local amplification of Rayleigh waves in the continental United States observed on the USArray. *Earth and Planetary Science Letters*, *402*, 50–57.

Foster, A., Ekström, G., & Hjörleifsdúttir, V. (2014). Arrival-angle anomalies across the USArray Transportable Array. *Earth and Planetary Science Letters*, *402*(Supplement C), 58–68.

Furumura, M., Kennett, B., & Furumura, T. (1998). Anomalous surface waves associated with deep earthquakes, generated at an ocean ridge. *Geophysical Journal International*, *134*(3), 663–676.

Harmon, N., Forsyth, D., & Webb, S. (2007). Using ambient seismic noise to determine short-period phase velocities and shallow shear velocities in young oceanic lithosphere. *Bulletin of the Seismological Society of America*, *97*(6), 2009–2023.

IRIS DMC (2010). Data services products: GMV, the USArray ground motion visualization. https://doi.org/10.17611/DP/USAGMV.1

Komatitsch, D., Vilotte, J.-P., Cristini, P., Labarta, J., Le Goff, N., Le Loher, P., et al. (2012). SPECFEM2D v7.0.0.

Levander, A. R. (1990). Seismic scattering near the Earth's surface. *Pure and Applied Geophysics*, *132*(1), 21–47. https://doi.org/10.1007/BF00874356

Lin, F., & Ritzwoller, M. (2011). Helmholtz surface wave tomography for isotropic and azimuthally anisotropic structure. *Geophysical Journal International*, *186*, 1104–1120.

Lin, F.-C., Tsai, V. C., & Ritzwoller, M. H. (2012). The local amplification of surface waves: A new observable to constrain elastic velocities, density, and anelastic attenuation. *Journal of Geophysical Research*, *117*, B06302. https://doi.org/10.1029/2012JB009208

Maeda, T., Furumura, T., & Obara, K. (2014). Scattering of teleseismic *P*-waves by the Japan trench: A significant effect of reverberation in the seawater column. *Earth and Planetary Science Letters*, *397*, 101–110.

Sun, D., & Helmberger, D. (2011). Upper-mantle structures beneath USArray derived from waveform complexity. *Geophysical Journal International*, *184*(1), 416–438.

Yu, C., Zhan, Z., Hauksson, E., & Cochran, E. (2017). Strong *SH*-to-love wave scattering off the Southern California continental borderland. *Geophysical Research Letters*, *44*, 10,208–10,215. https://doi.org/10.1002/2017GL075213